Electronic Supplementary Material (ESI) for Inorganic Chemistry Frontiers.

Surface Immobilization of Nitrogen-coordinated Iron Atom – A Facial and Efficient Strategy toward MNC Site with Superior Catalytic Activity

Qiankun Hou, Nan Yang, Kang Liu, De Ding, Yongpeng Lei, Min Liu, Yin Chen*

[1] Central South University, College Chemistry & Chemical Engineering, Changsha 410083, Hunan, China

[2] Central South University, School of Physics & Electronic, Changsha, Hunan, China

[3] Shaanxi Electric Power Research Institute, Xi'an 710054, Shanxi, China

[4] Central South University, Powder Met Res Inst, Changsha 410083, Hunan, China

† These authors contribute equally.

Contents

General procedure, powder XRD, IR, Raman, XPS, UV-Vis, TGA, XANES, SEM images, TEM images, electro-chemical analysis, Tables S1-S3, Figures S1-S23.

Material Synthesis and Characterization:

Chemicals:

Cobalt nitrate hexahydrate ($Co(NO_3)_2•6H_2O$,99%), Tris(2,2'-bipyridine)iron(II) hexafluorophosphate, Triphenylbenzene, Acetyl chloride, Nafion, RuO_2 and commercial Pt/C (20 wt% metal) were purchased from Aladdin Industrial Corporation. All the chemicals were used without further purification.

The preparation of 1,3,5-Benzenetribenzoic acid

Under the condition of ice water bath, 33g (0.25 mol) anhydrous aluminum trichloride was dissolved in 180 ml acetyl chloride under stirring condition. 10 g (0.03 mol) triphenylbenzene was dissolved in 200 ml of dichloromethane, and then slowly added into the aluminum trichloride solution via a dropping funnel. With the addition of triphenylbenzene, the mixture gradually becomes reddish brown. After reacting for 3 h at room temperature, the mixture was slowly poured into a beaker filled with ice water under vigorous stirring, and reacted overnight to obtain a yellow slurry. The yellow slurry was extracted by dichloromethane, and the obtained organic layer was dried. Crude product was obtained by removing the solvent, which was further washed with ethanol to afford pure 1,3,5-tris (4-acetylphenyl) benzene with a yield of 85%.

Then, 11 g (25 mmol) 1,3,5-tris (4-acetylphenyl) benzene was dissolved in 500 ml 1,4-dioxane. 35 g (0.87 mol) sodium hydroxide was dissolved in 240 ml of ice water, and then 10 ml liquid bromine was slowly dropped into it with stirring. The resulting sodium hypobromite solution is slowly added to the 1,3,5-tris (4-acetylphenyl) benzene solution. A yellow suspension was formed and stirred at 60 ^{o}C for another 2h, then cooled to room temperature. The reaction was quenched by the addition of a 5% sodium thiosulfate solution. White 1,3,5-Benzenetribenzoic acid was afforded after hot filtration and acidification treatment with a yield of 78%. mp > 300 ^{o}C; ^{1}H NMR (300 MHz, DMSO) (Figure S23, S24) δ 13.1 (bs, 3H), 8.1 (m, 15H); ^{13}C NMR (75 MHz, DMSO) δ 167.6, 144.3,141.2,130.5, 130.4, 127.9, 126.1.

Preparation of Co(BTB)

$Co(NO)_3 \cdot 6H_2O$ (218.8 mg, 0.75 mmol), 1,3,5-Benzenetribenzoic acid (H_3BTB, 76.7 mg, 0.18 mmol) were added into a 100 mL thick-walled Schlenk flask, then was dissolved with 50 ml N,N-dimethylformamide (DMF) under sonication. The transparent solution was reacted under 105 ^{o}C for 36 h, the as-prepared reddish precipitate was filtrated and washed for three times, then dried at 90 ^{o}C under vacuum to afford 89 mg Fe(bpy)-Co(BTB) crystal (yield: 80%). Based on the single crystal strucuture, the chemical formula of the crystal is $Co_{11}(BTB)_6(NO_3)_4(DMF)_x(H_2O)_y$.

Structural characterization:

The single crystal data were collected on a Bruker APEX-II CCD model with Cu Kα radiation (λ=1.5406Å). The XRD results were recorded on a Rigaku RU-200b X-ray powder diffractometer (XRD) with Cu Kα radiation (λ=1.5406 Å), 2-theta was run from 5^{o} to 75^{o} with a scan speed of 0.25^{o}/s. NMR spectra were recorded on Bruker Avance III HD 400MHz spectrometers. Inductively Coupled Plasma Optical Emission Spectrometry (ICP-OES) measurements were recorded on a PerkinElmer NexION 300X model. Infrared spectra (transmission) were recorded on a Nicolet Magna 6700 FT spectrometer equipped with a cell under controlled atmosphere. Raman spectra were recorded on a Renishaw inVa Raman microscope with an Arion laser at the excitation wavelength of 532 nm. Scanning electron microscopy (SEM) images were taken on Nova Nano SEM 450. TEM (Hitachi-7700, 100KV) were used to investigate the morphology and microstructure. Specific surface area (BET) were tested on a Micromeritics ASAP 2020 model. For TEM investigations, the samples were dispersed in ethanol by ultrasonication. A drop of suspension was then placed on a 200-mesh Cu grid support, which was dried in a vacuum oven at room temperature for 4 h. X-ray photoemission spectroscopy experiments (XPS) were perfomed on the Thermo Fisher Scientific ESCALAB 250Xi XPS System. Thermogravimetric analysis (TGA) measurements were carried out on a TA SDT Q600 thermal analyzer heating from room temperature to 600℃ at the rate of 5℃ min $^{-1}$ in nitrogen .

The X-ray absorption find structure spectra (Co K-edge) were obtained at beamlines 01C1 of the National Synchrotron Radiation Research Center (NSRRC,

Taiwan), the data collection were carried out in transmission/fluorescence mode using ionization chamber. All spectra were collected in ambient conditions.

XAFS Analysis and Results

The acquired EXAFS data were processed according to the standard procedures using the ATHENA module implemented in the IFEFFIT software packages. The k^3-weighted EXAFS spectra were obtained by subtracting the post-edge background from the overall absorption and then normalizing with respect to the edge-jump step. Subsequently, k^3-weighted $\chi(k)$ data of Co K-edge were Fourier transformed to real (R) space using a handing window (dk=1.0 $Å^{-1}$) to separate the EXAFS contributions from different coordination shells. To obtain the quantitative structural parameters around central atoms, least-squares curve parameter fitting was performed using the ARTEMIS module of IFEFFIT software packages.

Electrochemical measurements:

Electrochemical experiments were carried out using the ZAHNER electrochemical workstation (Germany) with a three-electrode system in 1.0M KOH. A glassy carbon (GC) RDE of 4 mm in diameter coated with the catalyst ink was used as the working electrode, Pt plate as counter electrode, and saturated calomel electrode (SCE) as reference electrode. RHE was used in this work. RHE was used in this article, E (RHE) = E (SCE) +0.2412 + 0.059×pH. Prior to test, the electrolyte was bubbled with O_2 or N_2 for 30 min to make sure that the O_2 in the solution was saturated.

All the cyclic voltammetry (CV) tested in O_2 saturated 1.0 M KOH under room temperature with a sweep rate of 5 mV s^{-1}. Catalytic activity toward the OER was evaluated from 0 V to 1.0 V vs. RHE, and the performance of ORR was investigated from 1.0 V to 1.9V vs. RHE.

Linear-sweep voltammetry measurements were performed at a rotation speed of 1600 rpm at a scan rate of 10 mV/s to get rid of the bubbles. Cyclic voltammograms (CVs) were conducted at a rotation rate of 1600 rpm at a scan rate of 50 mV/S. All polarization curves were iR corrected.

Table S1. Crystal Structure and Refinement Datasheet

Compound	**Co(BTB)**
Empirical formula	$C_{162}H_{92}Co_{11}O_{60}$ [+solvent]
Formula weight	3646.59
Temperature(K)	213(2)
Crystal system	Monoclinic
Space group	C 2/c
a [Å]	47.157(2)
b [Å]	37.345(2)
c [Å]	33.801(4)
α [deg]	90
β [deg]	97.1
γ [deg]	90
V[Å^3]	59068(5)
Z	4
ρ [g/cm3]	0.867
F(000)	7588
Crystal size [mm^3]	0.100 x 0.100 x 0.100
Theta range for data collection	1.677 to 50.004°.
Index ranges	-53<=h<=53, -42<=k<=41, -38<=l<=38
Reflections collected	366169
Refinement method	Full-matrix least-squares on F2
Data / restraints / parameters	45744 / 1791 / 906
Goodness-of-fit	1.104
R1,wR2 [I>2σ(I)]	0.1097, 0.1940
R1,wR2 (all data)	0.2742, 0.3146

Table S2. Fe K-edge EXAFS Parameters for Surface Fe samples

Sample	Neighboring atom of Ni	N [a]	R (Å) [b]	σ^2 (Å$^2\cdot10^{-3}$) [c]	ΔE0 (eV) [d]	*R* factor (%)
$Fe(bpy)_{10}$-MOF-177	N	6.10	2.012	0.0089	0.2217	0.032
FeN_x-MOF-177	N	5.27	2.005	0.0116	0.0036	0.076

[a] *N*: coordination numbers; [b] *R*: bond distance; [c] σ^2: Debye-Waller factors; [d] ΔE_0: the inner potential correction. *R* factor: goodness of fit.

Table S3. Summary of the compositions in Co(BTB) samples determined by XPS.

	C (At.%)	N (At.%)	O (At.%)	Co (At.%)	Fe (At.%)
Co(BTB)	68.33	/	24.89	6.78	/
$Fe(bpy)_{10}$-MOF-177	58.16	13.05	21.82	4.87	2.28
FeN_x-MOF-177	56.98	11.71	23.68	5.24	2.39

Table S4: The comparison of OER performance of different Fe-based catalysts

Catalyst	Overpotential @10mA/cm^{-2}(mV)	Tafel slope [mV dec^{-1}]	Ref.
FeN_x-embedded PNC	395	80	[1]
Fe-N_4 SAs/NPC	430	95	[2]
CeO_2-FeNC-5	327	81	[3]
FeNP@Fe-N-C	340	216	[4]
CoNP@FeNC-0.05	400	146	[5]
Fe/Fe_3C-F@CNT	286	42	[6]
AFC-MOFs (1 : 4)	256	42.7	[7]
2D MOF-Fe/Co(1:2)	238	52	[8]
Fe_1Co_2-P/C	362	50.1	[9]
Co/Fe (1:1)-MOF	317	42	[10]
$(Fe(II)_1Fe(III)_1)_{0.6}$/NMOF-Co	330	50	[11]
FeN_x-Co(BTB)	261	27	This work

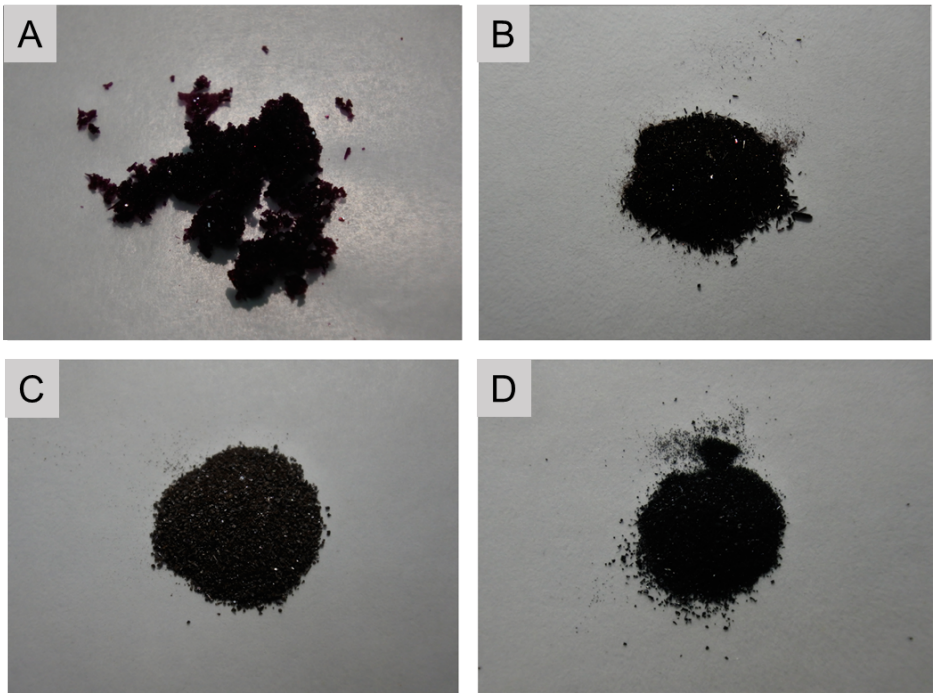

Figure S1 : Photos of (A) Co(BTB); (B) $Fe(bipy)_3(PF_6)_2$; (C) $Fe(bpy)_{10}$-Co(BTB)；(D) FeN_x-Co(BTB).

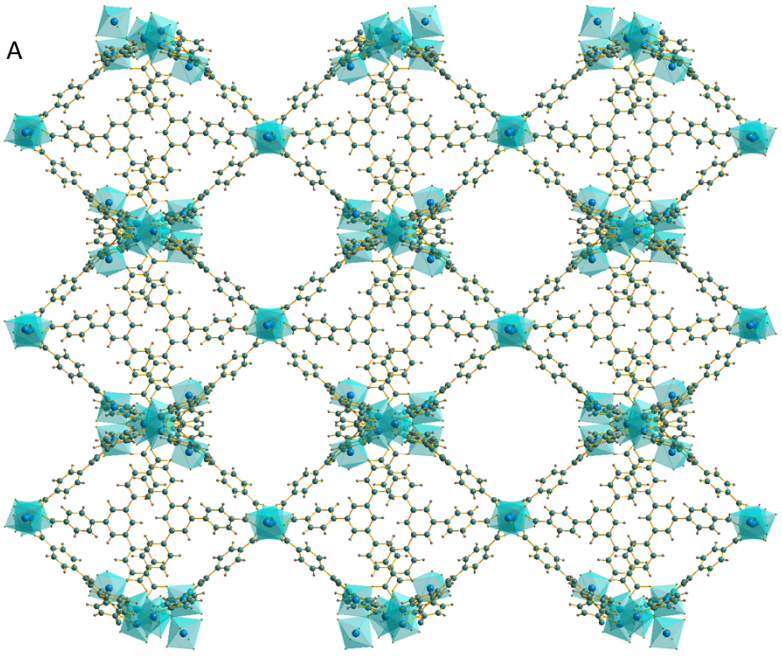

B

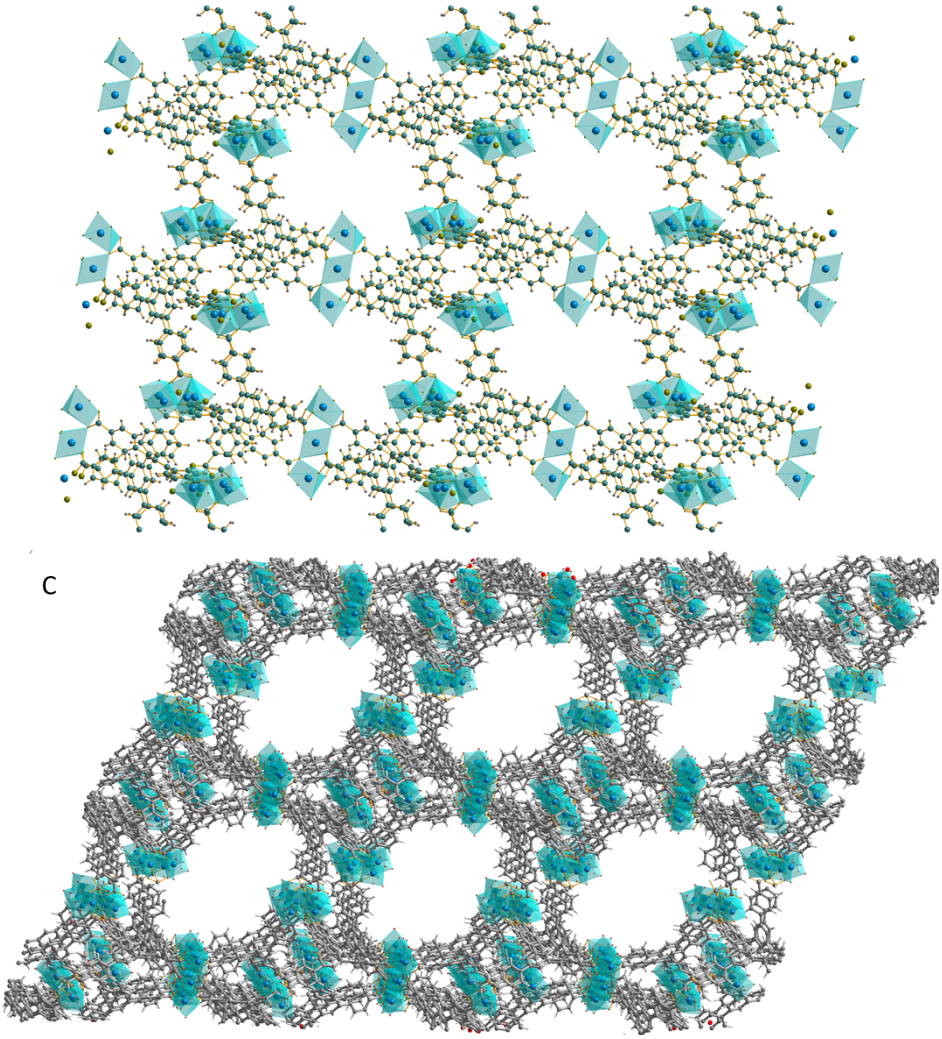

Figure S2: Crystal structure of Co(BTB). Architecture structure of Co(BTB) lattice alone c-axis (A) with rhombus channels; alone b-axis (B); alone 200 plane (C).

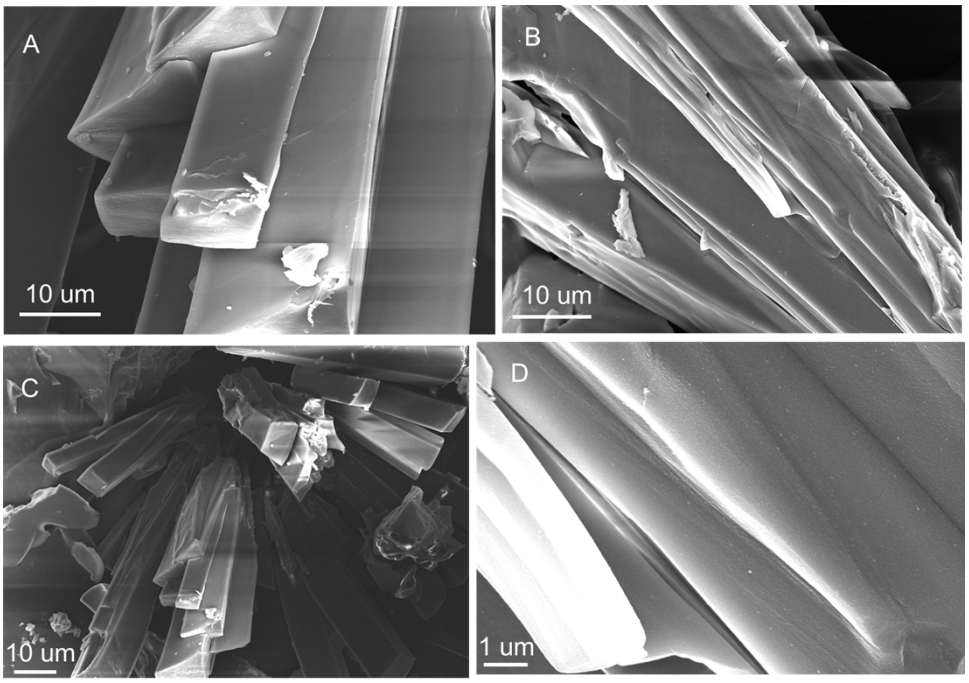

Figure S3 : SEM images of (A), (B) Co(BTB); (C), (D) $Fe(bpy)_{10}$-Co(BTB).

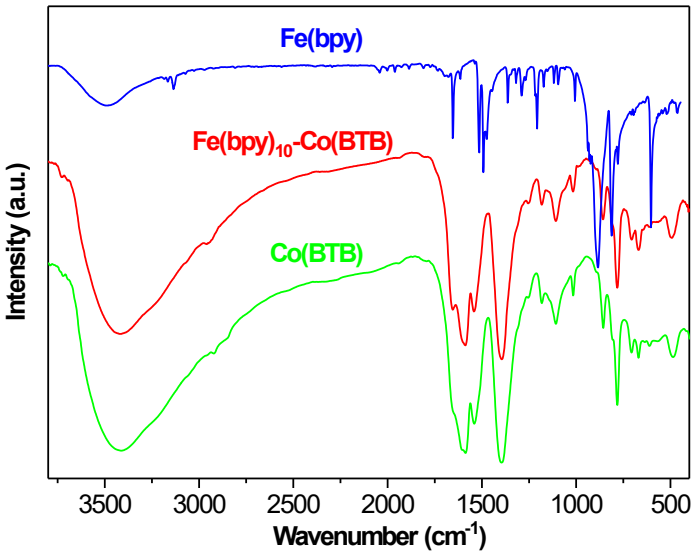

Figure S4 : Comparison of FT-IR spectra of Fe(bpy), Co(BTB) and $Fe(bpy)_{10}$-Co(BTB).

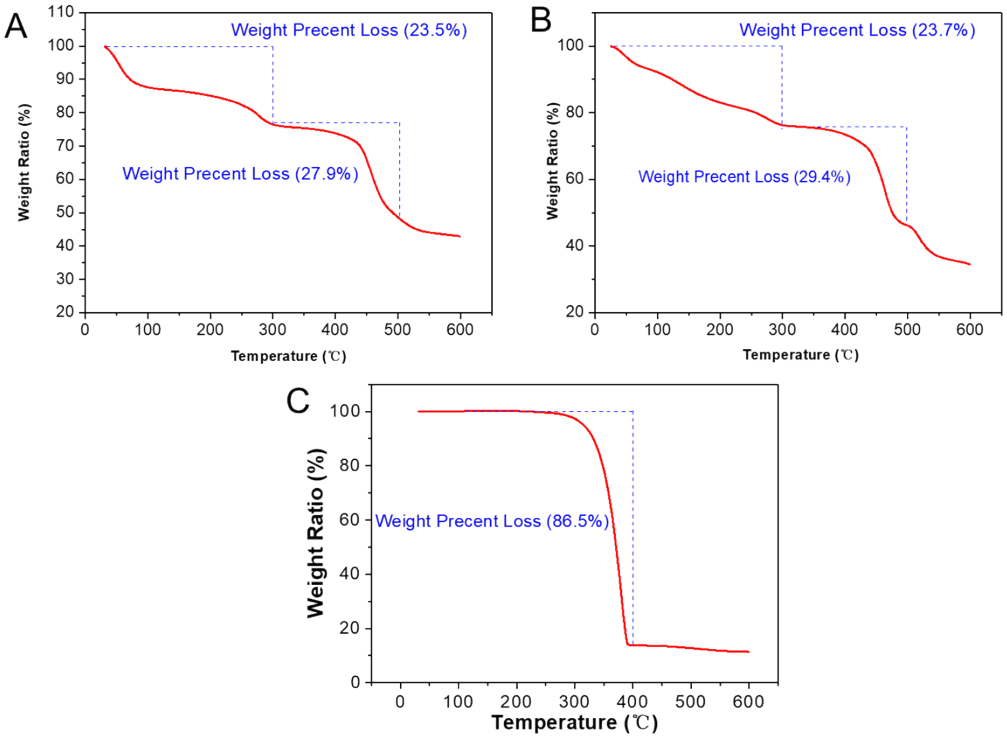

Figure S5. TGA of (A) Co(BTB); (B) $Fe(bpy)_{10}$-Co(BTB); (C) $Fe(bipy)_3(PF_6)_2$ under N_2 from 25°C to 600 °C with a heating rate of 20 °C/min

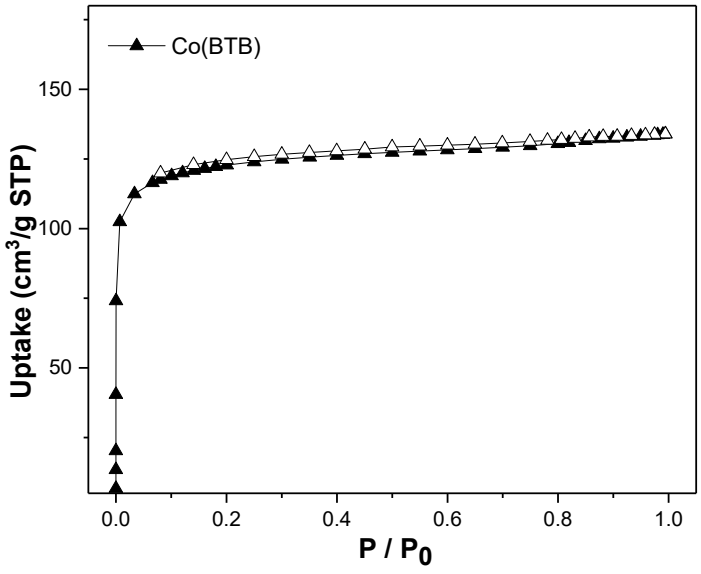

Figure S6: N_2 adsorption-desorption isotherms of **Co(BTB)** (black) at 77 K and various pressures up to 1 bar.

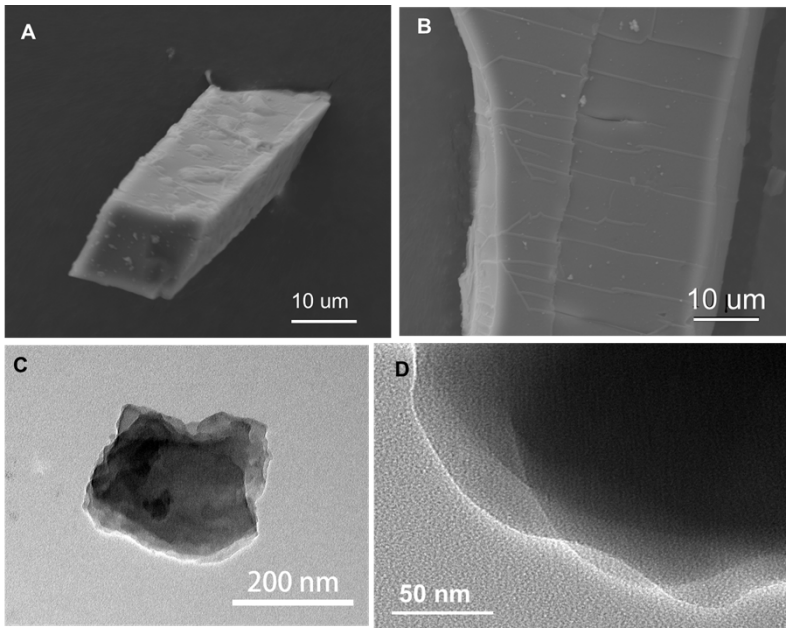

Figure S7: SEM images (A), (B) and TEM images(C), (D) of FeN_x-Co(BTB).

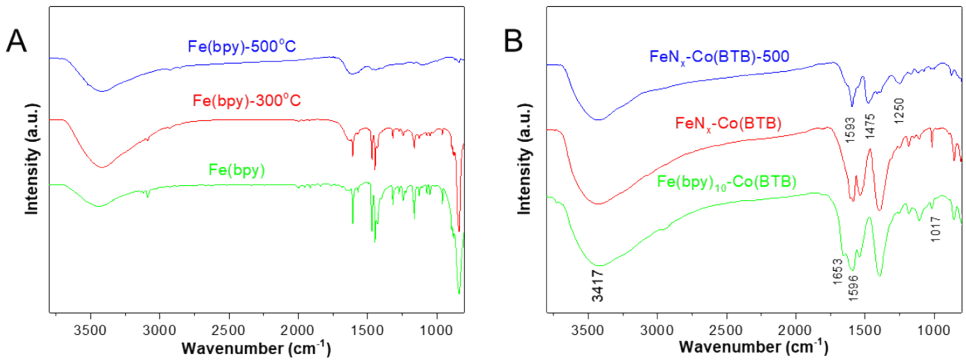

Figure S8: IR spectra of (A) $Fe(bipy)_3(PF_6)_2$ and (B) $Fe(bpy)_{10}$-Co(BTB) treated under diffrent temperature

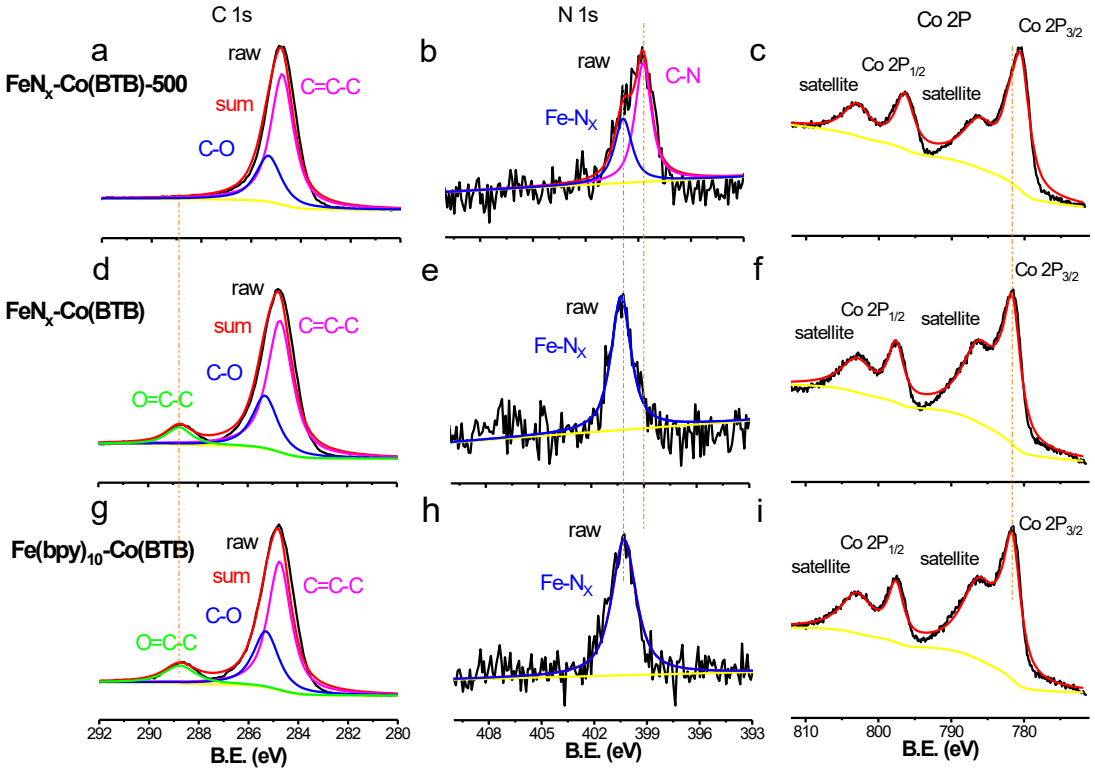

Figure S9: Comparation of C 1s, N 1s, Co 2p XPS spectra for $Fe(bpy)_{10}$-Co(BTB), FeN_x-Co(BTB) and FeN_x-Co(BTB)-500.

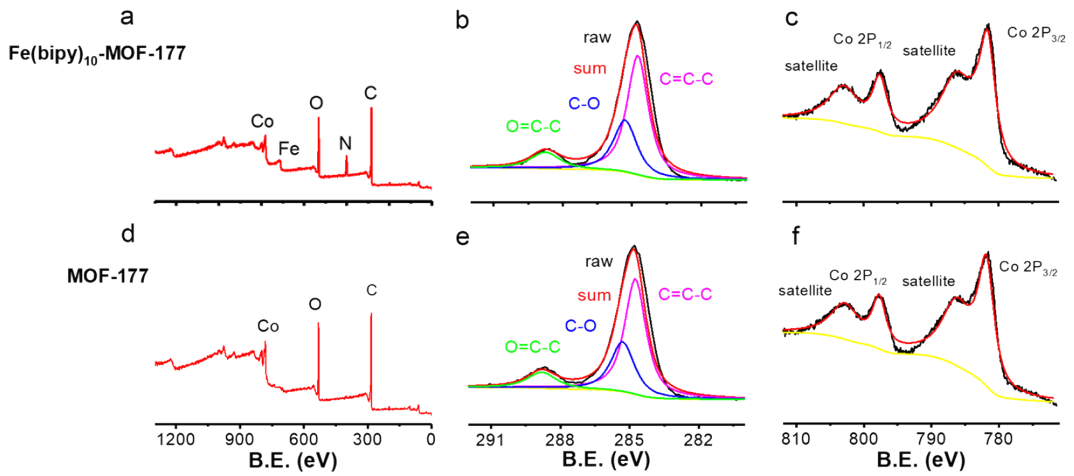

Figure S10: Comparation of C 1s, N 1s, Co 2p XPS spectra for Co(BTB) and $Fe(bpy)_{10}$-Co(BTB).

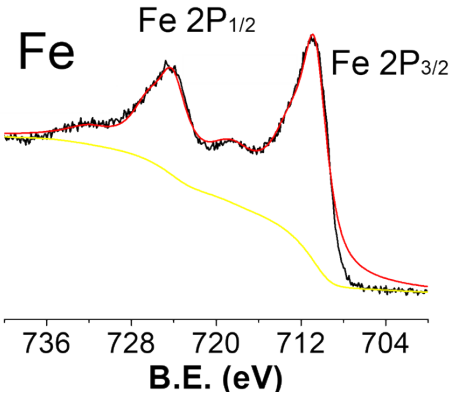

Figure S11 : Fe 2p XPS spectra for $Fe(bpy)_{10}$-Co(BTB).

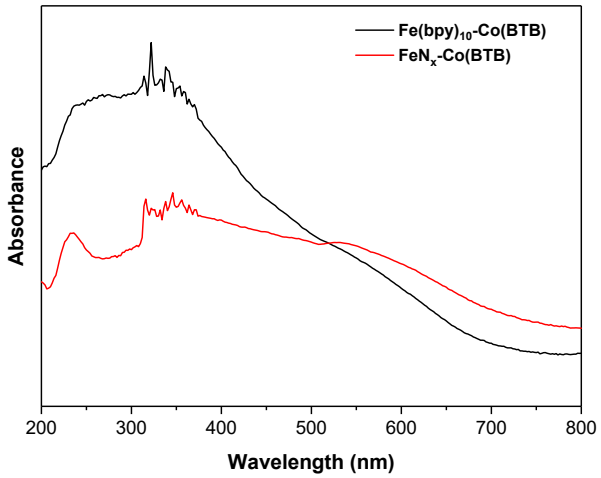

Figure S12: Powder diffuse reflection UV-Vis spectra of $Fe(bpy)_{10}$-Co(BTB) and FeN_x-Co(BTB).

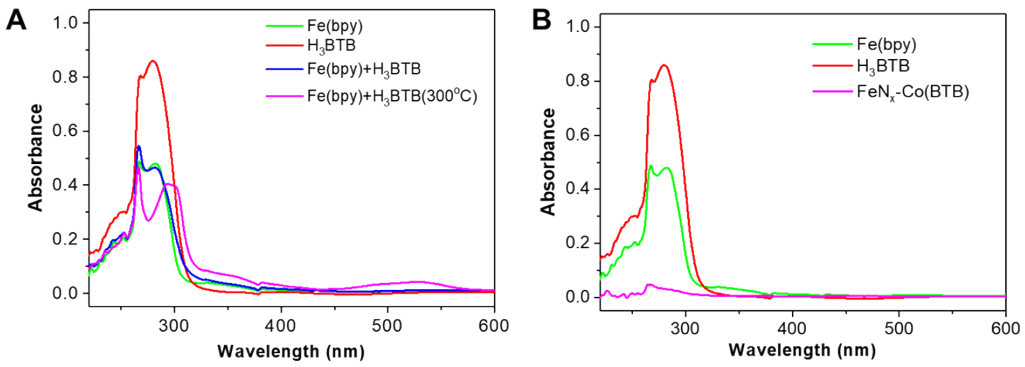

Figure S13: (A) UV-Vis spectra of Fe(bpy), H_3BTB, the mixture of Fe(bpy) and H_3BTB, the thermal treated mixture in solution; (B) UV-Vis spectra of Fe(bpy), H_3BTB solution and the acetone leach solution of FeN_x-Co(BTB).

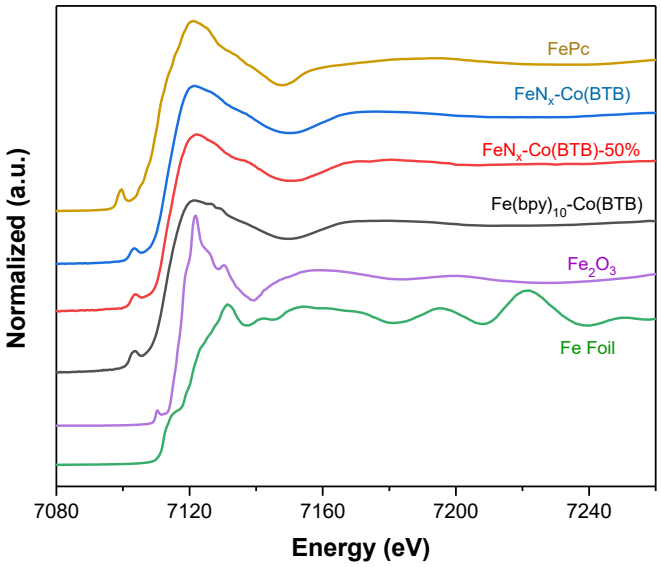

Figure S14: Normalized Ni K-edge XANES spectra of Fe Foil, Fe_2O_3 and Co(BTB) samples.

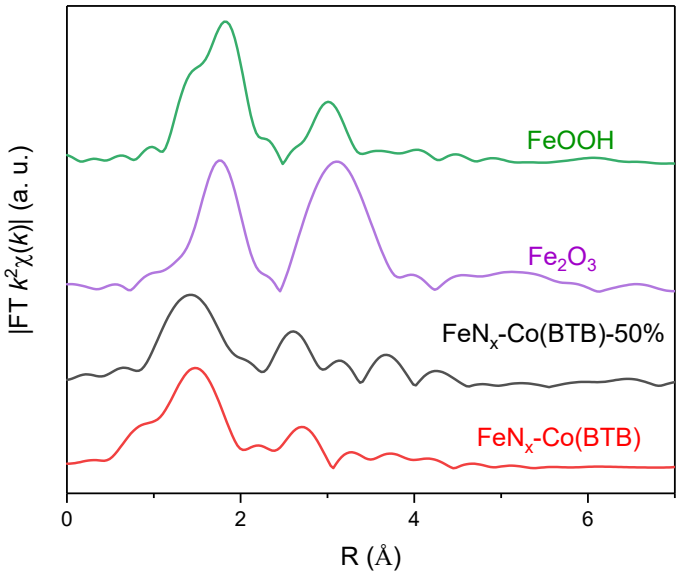

Figure S15: Fourier transformed magnitudes of the experimental Fe K-edge EXAFS signals of FeN_x-Co(BTB) along with reference samples.

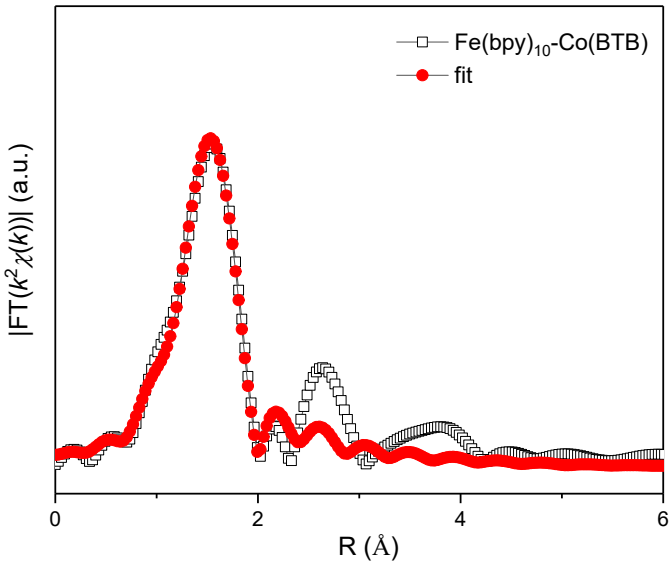

Figure S16: Fe K-edge EXAFS fitting curve for $Fe(bpy)_{10}$-Co(BTB).

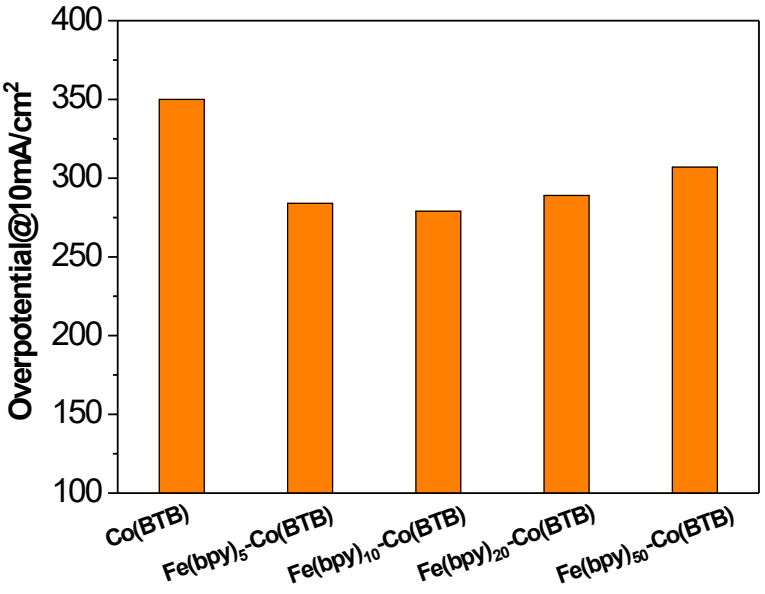

Figure S17: The overpotentials for Co(BTB) samples with different Fe(byp) content at current density of 10 mA cm^{-2}.

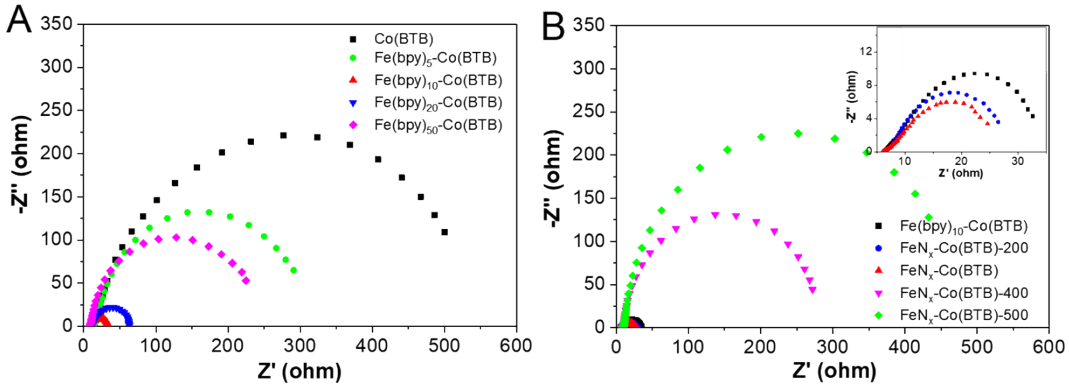

Figure S18: (A) EIS Nyquist plots of Co(BTB) samples with different Fe(byp) content at 1.57 V versus RHE. (B) EIS Nyquist plots of $Fe(bpy)_{10}$-Co(BTB) sample thermal treated under different temperatures at 1.57 V versus RHE.

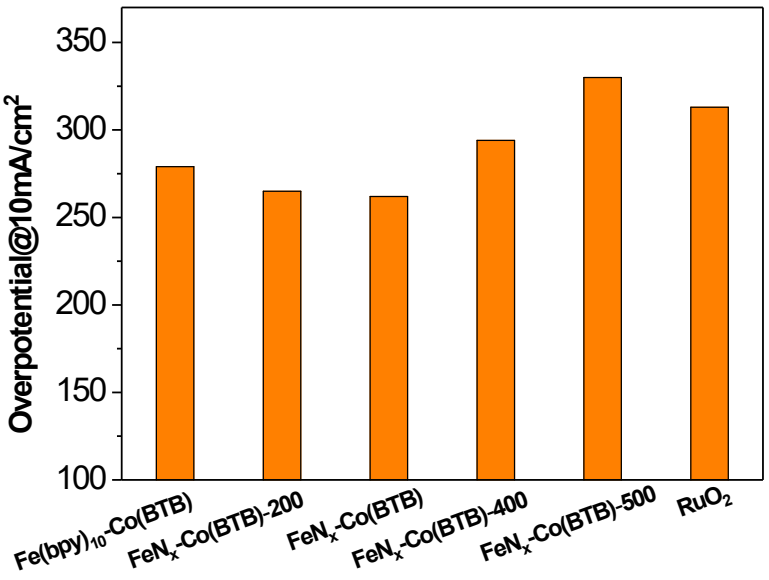

Figure S19: The overpotentials for $Fe(bpy)_{10}$-Co(BTB) sample thermal treated under different temperatures at current density of 10 mA cm^{-2}.

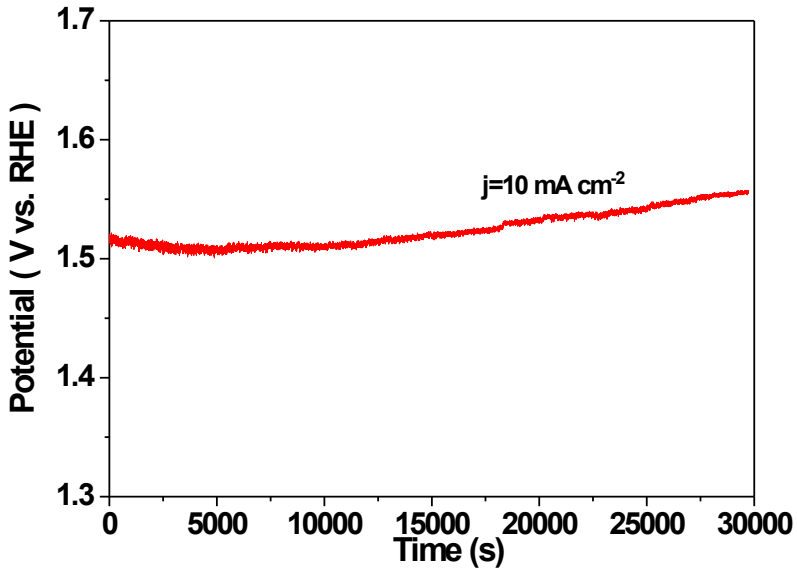

Figure S20: Time-dependent voltage curve of $Fe(bpy)_{10}$-Co(BTB) measured at an applied current density of 10mA/cm^{-2} in 1.0 M KOH solution.

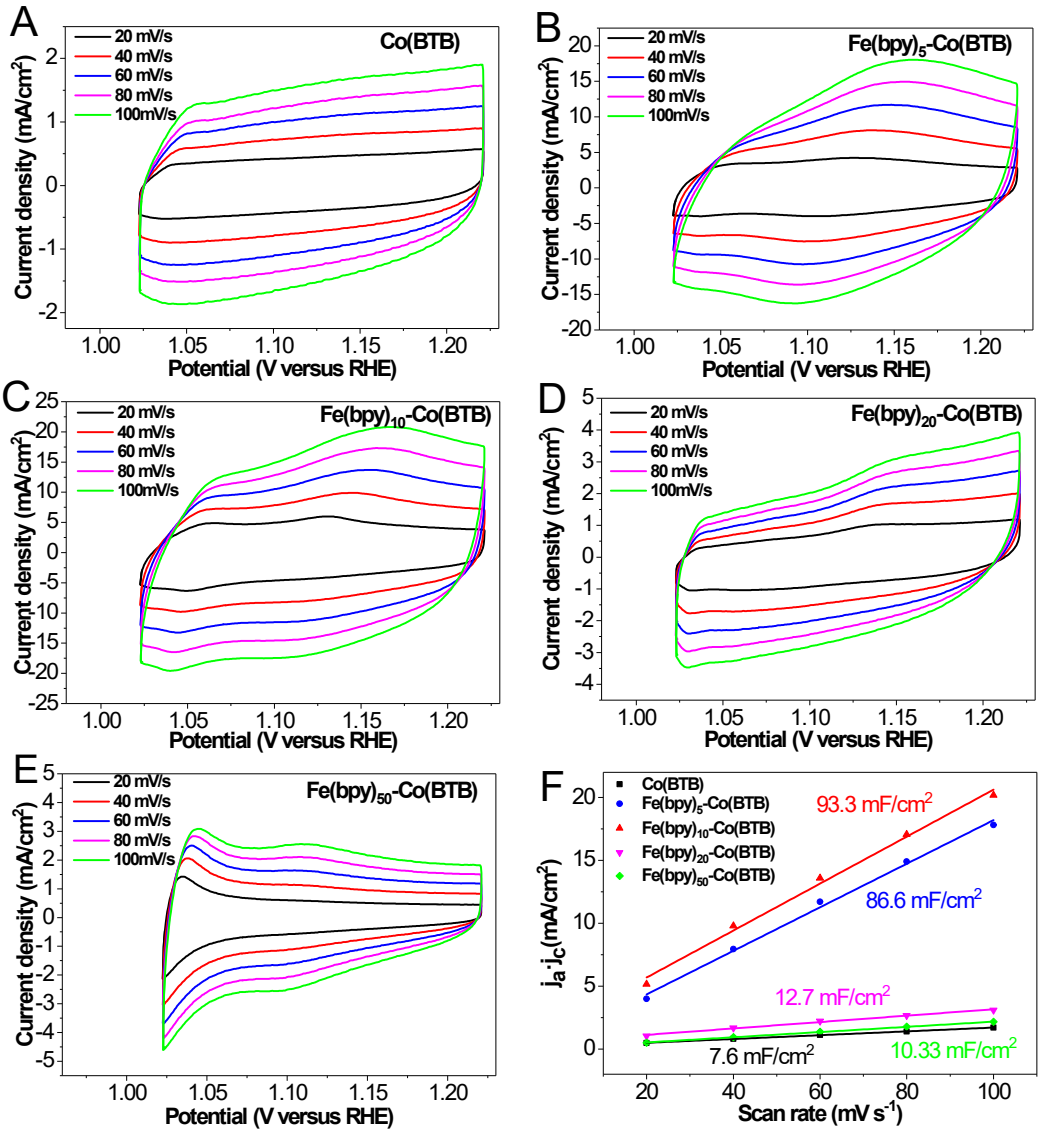

Figure S21. (a-e) The CV curves of Co(BTB) samples with different Fe(byp) content. (f) Comparison of electrochemical double-layer capacitances of corresponding samples.

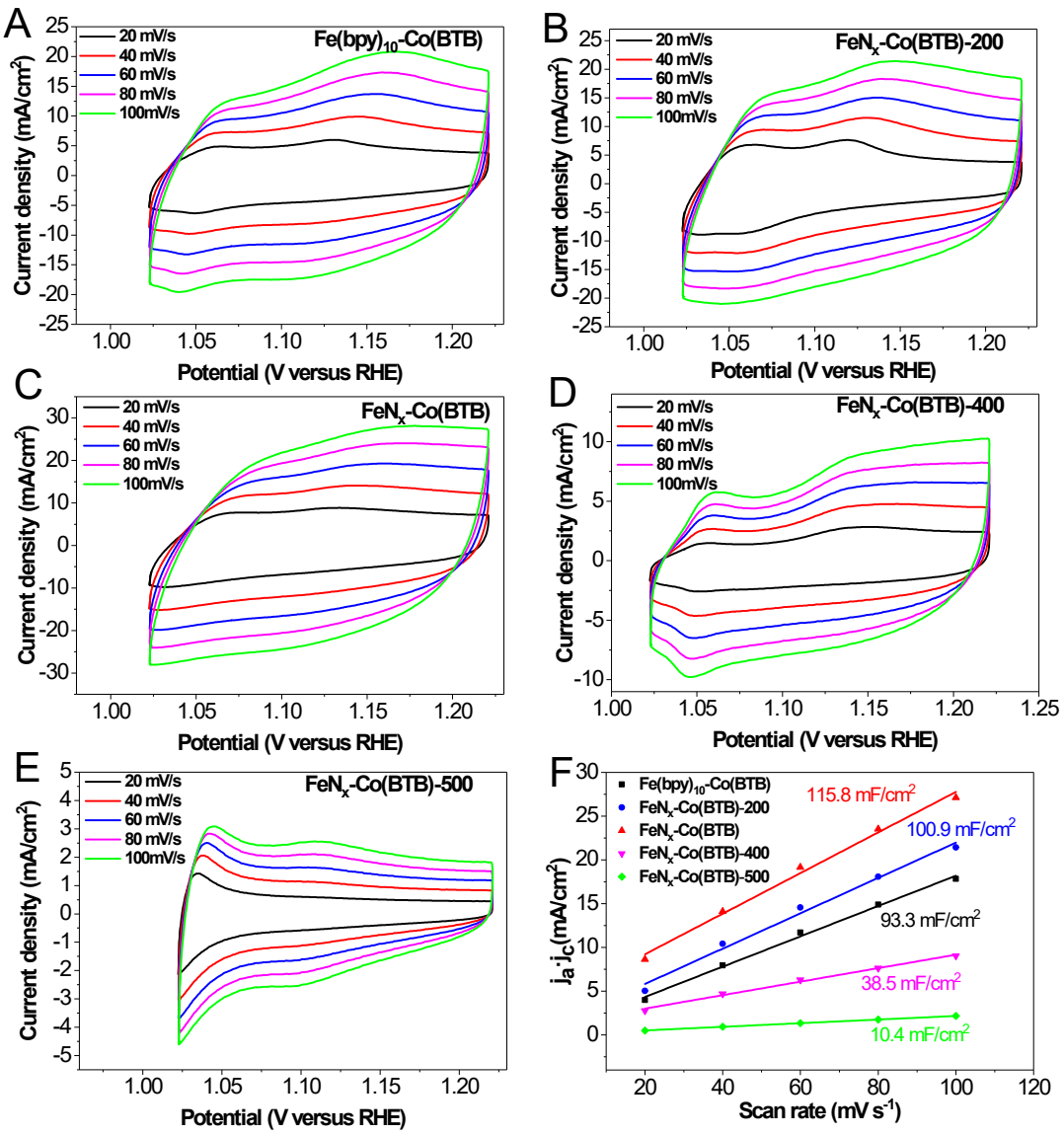

Figure S22. (a-e) The CV curves of $Fe(bpy)_{10}$-Co(BTB) sample thermal treated under different temperature. (f) Comparison of electrochemical double-layer capacitances of corresponding samples.

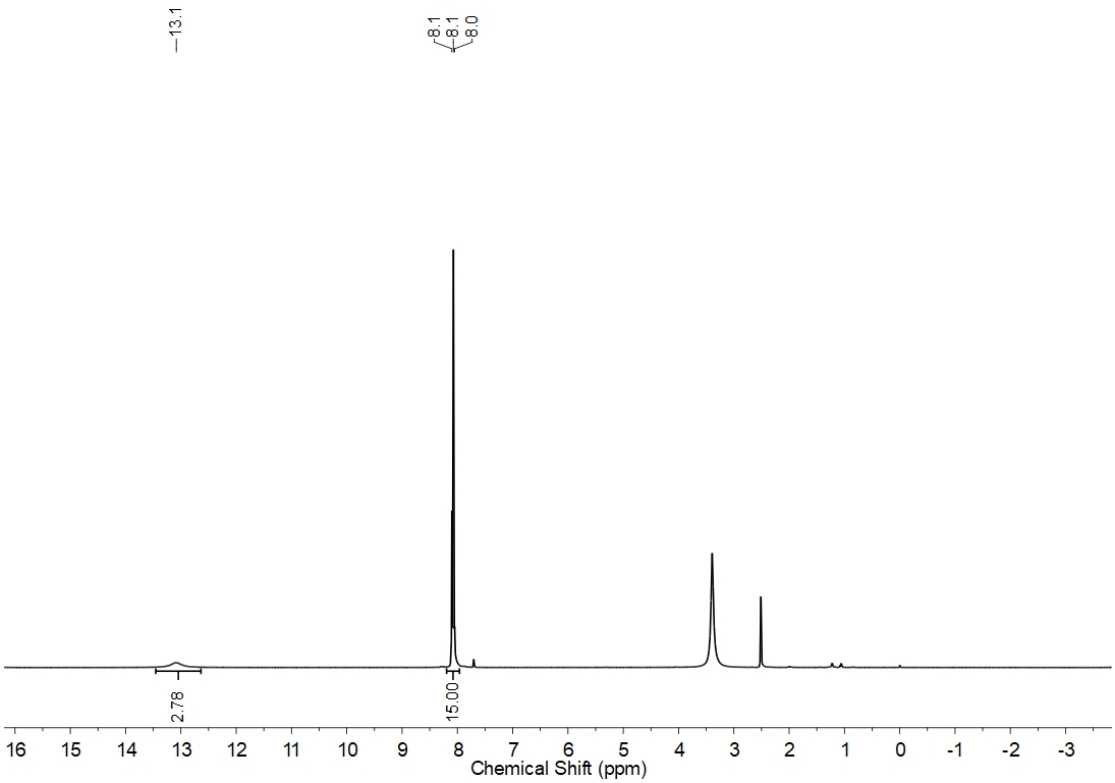

Figure S23. [1]H-NMR spectrum of 1,3,5-Benzenetribenzoic acid.

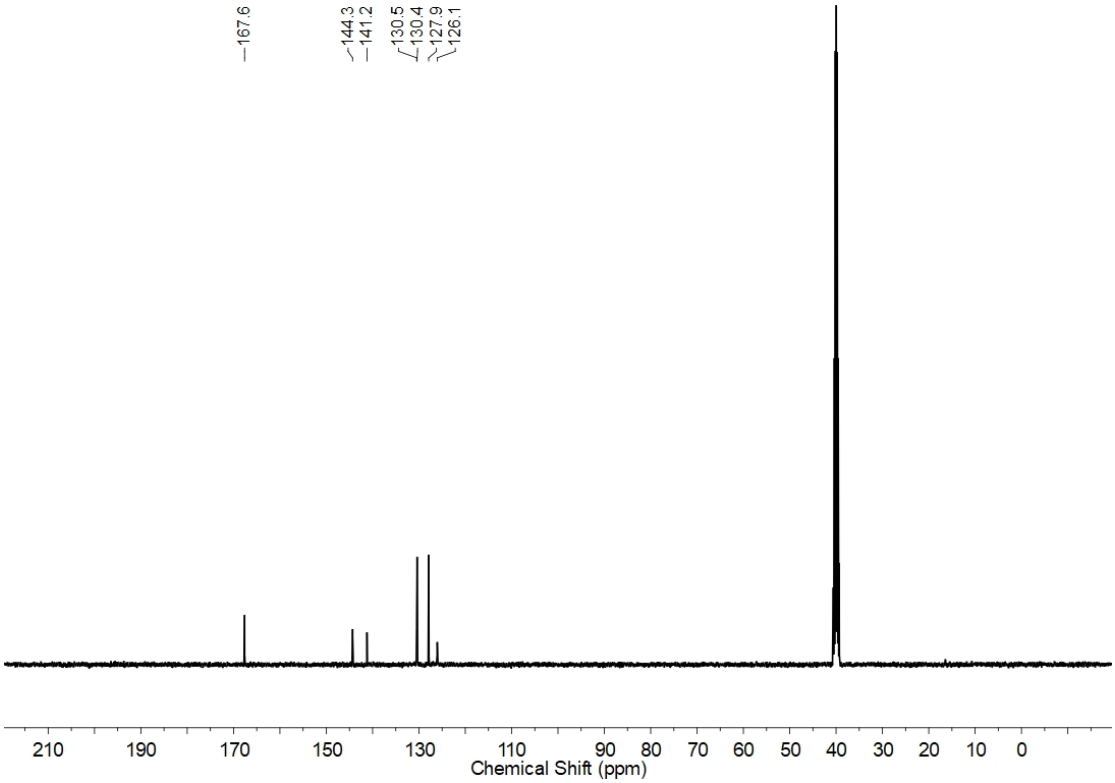

Figure S24. [13]C-NMR spectrum of 1,3,5-Benzenetribenzoic acid.

Reference:

1. L. Ma, S. Chen, Z. Pei, Y. Huang, G. Liang, F. Mo, Q. Yang, J. Su, Y. Gao, J. A. Zapien and C. Zhi, *ACS Nano*, 2018, **12**, 1949-1958.
2. Y. Pan, S. Liu, K. Sun, X. Chen, B. Wang, K. Wu, X. Cao, W.-C. Cheong, R. Shen, A. Han, Z. Chen, L. Zheng, J. Luo, Y. Lin, Y. Liu, D. Wang, Q. Peng, Q. Zhang, C. Chen and Y. Li, *Angewandte Chemie International Edition*, 2018, **57**, 8614-8618.
3. Y. Huang, Y. Zhang, J. Hao, Y. Wang, J. Yu, Y. Liu, Z. Tian, T.-S. Chan, M. Liu, W. Li and J. Li, *Journal of Colloid and Interface Science*, 2022, **628**, 1067-1076.
4. C. Yang, S. Shang, Q. Gu, J. Shang and X.-y. Li, *Journal of Energy Chemistry*, 2022, **66**, 306-313.
5. Y. Xue, Y. Guo, Q. Zhang, Z. Xie, J. Wei and Z. Zhou, *Nano-Micro Letters*, 2022, **14**, 162.
6. T. Gao, C. Zhou, Y. Zhang, Z. Jin, H. Yuan and D. Xiao, *Journal of Materials Chemistry A*, 2018, **6**, 21577-21584.
7. Q. Zhao, X. Lin, J. Zhou, C. Zhao, D. Zheng, S. Song, C. Jing, L. Zhang and J.-Q. Wang, *European Journal of Inorganic Chemistry*, 2021, **2021**, 702-707.
8. K. Ge, S. Sun, Y. Zhao, K. Yang, S. Wang, Z. Zhang, J. Cao, Y. Yang, Y. Zhang, M. Pan and L. Zhu, *Angewandte Chemie International Edition*, 2021, **60**, 12097-12102.
9. W. Hong, M. Kitta and Q. Xu, *Small Methods*, 2018, **2**, 1800214.
10. Y. Pan, J. Zhang, Z. Zhao, L. Shi, B. Wu and L. Zeng, *International Journal of Hydrogen Energy*, 2021, **46**, 34565-34573.
11. M. Zhao, T. Guo, W. Qian, Z. Wang, X. Zhao, L. Wen and D. He, *Chemical Engineering Journal*, 2021, **422**, 130055.